ACS OMEGA

Open Access

http://pubs.acs.org/journal/acsodf

Article

Biotemplate-Assisted Growth of ZnO in Gas Sensors for ppb-Level NO_2 Detection

Jia-Cheng Jian, Yu-Chi Chang,* Sheng-Po Chang, and Shoou-Jinn Chang

Cite This: *ACS Omega* 2024, 9, 1077−1083

Read Online

ACCESS | Metrics & More | Article Recommendations

ABSTRACT: With the growing concern over the adverse effects of environmental pollution on human health, the combination of environmentally friendly and nontoxic biomaterials with metal oxide semiconductor materials for electronic devices has emerged as a prominent trend in current research. In this study, we utilized 150 mg apple biotemplates to assist in the hydrothermal synthesis of ZnO nanospheres. It successfully achieved high sensitivity for detecting 35 and 350 ppb NO_2 at room temperature, with responses of 13.74 and 132.44%, respectively. Simultaneously, the 5-cycle repeatability and multiple-gas selectivity exhibited significant improvements. The ZnO nanospheres demonstrated enhanced sensing performance compared to pure ZnO nanorods, which is attributed to the following mechanisms: reason I, the modified surface morphology increasing the surface-to-volume ratio; reason II, an increase in oxygen vacancies, leading to reduced crystallinity and a higher electron concentration; reason III, incorporation of carbon elements on the nanostructure surface to increase active sites. The novel gas sensor assisted by the apple pectin biotemplate offers a promising solution for NO_2 gas detection, featuring low operating temperatures, low concentrations, and high response sensitivity.

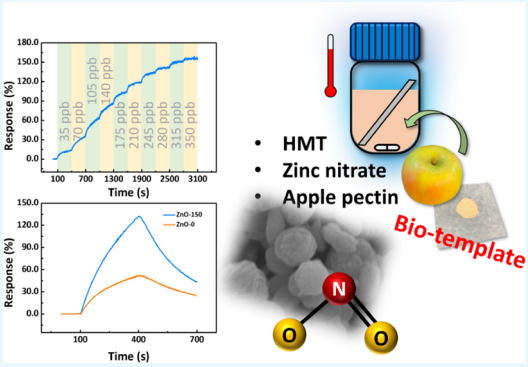

INTRODUCTION

Air pollution is a globally recognized and significant issue that poses severe implications for public health and the environment. In the 2015 World Health Assembly (WHA) held in Geneva, it was declared that both indoor and outdoor air pollution, particularly particulate matter, is considered one of the most critical environmental health risks worldwide.[1]

Among these pollutants, nitrogen dioxide (NO_2) is a prominent gaseous air pollutant composed of nitrogen and oxygen. It is formed when fossil fuels, such as coal, natural gas, petroleum, and diesel, are combusted at high temperatures. Even at trace gas concentrations, NO_2 can cause discomforting sensations like nausea, eye irritation, and skin itching.[2−4] Its harmful effects extend far beyond posing a threat to human health, as it interacts with other chemical compounds, leading to the formation of acid rain.

ZnO possesses a hexagonal wurtzite crystal structure, a wide band gap of 3.37 electron volts, high exciton binding energy, and excellent ultraviolet absorption properties and is nontoxic.[5,6] However, to address the low response and stability of pure ZnO in gas sensing applications, researchers have explored various strategies, such as altering the morphology,[7] establishing heterostructures with metal oxides,[8−10] decorating noble metal nanoparticles,[11] synthesizing binary metal oxide materials,[4] and employing biotemplates.[12−15] Additionally, enhancing carrier transport efficiency can be achieved through techniques such as heating the device or irradiating it with UV light during the measurement process.[16,17]

Biotemplates, known for their renewable and ecofriendly nature, are utilized to a significant effect. They offer excellent control over the surface morphology and size of nanostructures while facilitating the incorporation of carbon elements, which are critical factors in optimizing the gas sensing performance. Additionally, the biotemplate-assisted hydrothermal growth process is relatively straightforward and cost-effective, making it conducive to developing nontoxic products.[2,6,12,13,18−21]

In this research, apple pectin was utilized as a biotemplate to successfully synthesize ZnO nanospheres (ZnO-150) through a hydrothermal method. Comprehensive analyses of the physical and electrical properties of the sensing materials were performed. The investigation of electrical properties involved a detailed study of the working temperature and response of the gas sensing device. Subsequently, the sensitivity to NO_2 concentrations ranging from 35 to 350 ppb at room temperature was tested, the repeatability to NO_2 at 350 ppb

Received: September 21, 2023
Revised: November 30, 2023
Accepted: December 1, 2023
Published: December 28, 2023

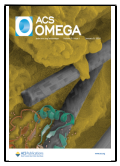

was examined, and the selectivity toward multiple gases (NO_2, C_2H_5OH, NH_3, and SO_2) was evaluated. Additionally, long-term stability tests were carried out. Based on all of the analyzed results, an explanation for the resistance variations was provided through theoretical mechanisms related to the observed factors.

EXPERIMENTAL SECTION

Synthesis of the ZnO Nanostructure. Figure 1 depicts a schematic representation of a synthesis process that utilizes

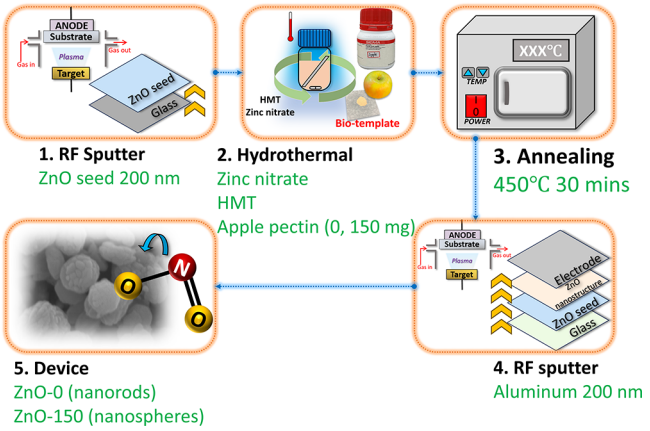

Figure 1. Schematic diagram illustrating the synthesis process of ZnO nanospheres using an apple pectin biotemplate for the fabrication of a NO_2 gas sensor device.

apple pectin. This process was employed to fabricate two distinct nanostructures: pure ZnO nanorods (denoted as ZnO-0) and ZnO nanospheres (denoted as ZnO-150). These structures were synthesized through a hydrothermal process, with the addition of 0 and 150 mg of the apple pectin biotemplate, respectively. Initially, the glass substrate was cleaned by sequentially immersing it in acetone, methanol, and DI water. This was followed by 10 min of ultrasonic oscillation, after which the substrate was dried with a nitrogen gun and placed in a circulating oven. A layer of 200 nm ZnO seeds was deposited onto the glass substrate by using RF sputtering.

The hydrothermal solution was prepared by dissolving 25 mM $Zn(NO_3)_2{\cdot}6H_2O$ and 25 mM hexamethylenetetramine (HMTA) in 100 mL of deionized water. Two variations were created: one with no apple pectin (0 mg) and the other with 150 mg of apple pectin (Uni-Onward Corp., New Taipei City, Taiwan). The solutions were heated to 95 °C and maintained at this temperature for 5 h to facilitate growth. Afterward, the samples were removed, washed with deionized water, dried using a nitrogen gun, and further dried in a circulating oven. To enhance crystal quality, the ZnO nanorods and nanospheres underwent rapid thermal annealing (RTA) at 450 °C for 10 min.

Characterization. The surface morphology of ZnO nanostructures was characterized by using scanning electron microscopy (SEM) and transmission electron microscopy (TEM). The crystal structure and lattice parameters were also measured by using TEM through the selected-area electron diffraction (SAED) technique. The distribution of elements was visualized through a 2D display of concentration using the element analysis method of EDS mapping. The crystal structure and preferred orientation were obtained by powder X-ray diffraction (XRD, Bruker D8D Plus-TXS, Cu KαI radiation (I = 1.5406 Å)). The characterization of inorganic and organic compounds on the surface was conducted by using X-ray photoelectron spectroscopy (XPS).

Electrical Measurement of Gas Sensors. In this section, NO_2, NH_3, SO_2, and C_2H_5OH were utilized as the sample gases. All of these sample gases were obtained through gas cylinders from suppliers. The concentration of each gas was diluted using nitrogen (N_2) gas, which is an inert gas and does not affect the reactions nor does it contain any moisture. The concentration of the gases introduced into the chamber was determined by analyzing them with commercially available calibration instruments corresponding to each specific gas.

The sensor devices' electrical properties were systematically measured using a Keithley 2400 power source in a stainless-steel chamber. The chamber maintained an air atmosphere with a relative humidity of 50−100% and a room temperature ranging from 25 to 27 °C. The devices were measured with a 0.1 V bias and positioned on a heater with a temperature range of 25−210 °C. The analyte gas was injected into the chamber via a microsyringe. The oxidative and reductive gas sensing responses of the sensor devices are characterized by the following equation (eq 1):

$$\text{Response} = \left| \frac{R_{gas} - R_{air}}{R_{air}} \right| \times 100\% \quad (1)$$

The process of depositing 200 nm-thick aluminum metal electrodes was carried out by using RF sputtering. The electrode pattern was defined as an interdigital-shaped structure that can be visualized as having a pair of five fingers. The interdigital width, length, and gap distance were 0.25, 4.5, and 0.25 mm, respectively. The total device area was 42.25 mm^2, and it was covered with an Al electrode of 18.75 mm^2.

RESULTS AND DISCUSSION

The surface morphologies of fabricated ZnO-0 and ZnO-150 were characterized using SEM. Figure 2a,b reveals the hydrothermal method employed with varying concentrations of the apple pectin biotemplate to achieve distinct surface morphologies. It is evident that the addition of apple pectin successfully modified the surface morphology, transforming the nanorods into nanospheres. The irregular nanospheres

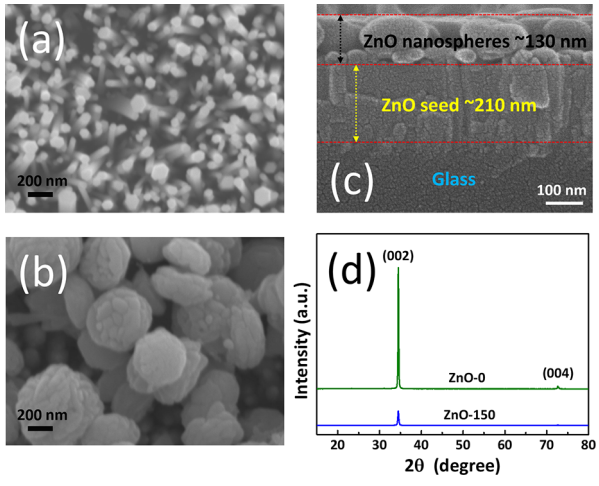

Figure 2. Surface morphology characterized by SEM images of (a) ZnO-0 and (b) ZnO-150. (c) SEM cross-sectional image of ZnO-150. (d) XRD spectra of ZnO-0 and ZnO-150.

https://doi.org/10.1021/acsomega.3c07280
ACS Omega 2024, 9, 1077−1083

exhibited an average diameter ranging from 250 to 450 nm (Figure 2b). In the cross-sectional image of ZnO-150 (Figure 2c), the thickness of the sensing film is approximately 130 nm, while the ZnO seed layer has a thickness of about 210 nm. XRD analysis was performed to investigate the phase identification and crystalline quality of the nanostructure. Comparing ZnO-0 and ZnO-150, subjected to annealing at 450 °C, the results are presented in Figure 2c. The obtained spectra revealed the presence of two crystal phases, namely, (002) and (004), with corresponding 2θ values of 34.5 and 72.6°, respectively. Notably, the intensity of the (002) peak indicated a strong preference for orientation along the (002) plane with the *c*-axis direction. These findings are consistent with the characteristic hexagonal wurtzite structure (JCPDS 36-1541). However, it was observed that the intensity of the (002) peak gradually decreased with adding apple pectin. This observation is consistent with previous research, which proposed that higher OH^- concentrations restrain preferential growth along the *c*-axis, resulting in the preservation of the spherical morphology and nanometric size in the primary particles.[22]

The biotemplate method was used to fabricate a single crystalline ZnO nanosphere, characterized by HR-TEM (Figure 3a). The crystal structure, crystallinity, and elemental

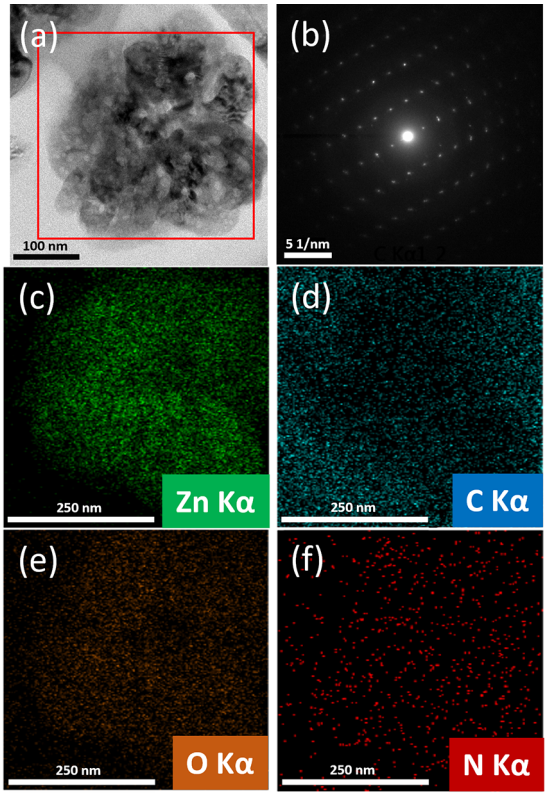

Figure 3. (a) HR-TEM image of the single ZnO nanosphere obtained by TEM; (b) SAED pattern; EDS mapping of (c) Zn, (d) C, (e) O, and (f) N.

concentrations were visualized by using the SAED and EDS mapping methods. The SAED analysis displayed the classification of single nanostructures with a lattice spacing of 0.236 nm, demonstrating that the ZnO nanostructures retained their single crystalline nature following biotemplate modification (Figure 3b). EDS mapping revealed the presence of Zn, C, and N elements (Figure 3c–f). It also confirmed the successful attachment of carbon elements to the ZnO nanospheres.

The existence of surface bonding in ZnO-0 and ZnO-150 was verified through the decomposition of XPS spectra for carbon, oxygen, and zinc elements by using the Gauss fitting procedure. The obtained fitting results are illustrated in Figure 4a. The high-resolution Zn 2p3 XPS spectra of ZnO-150 were

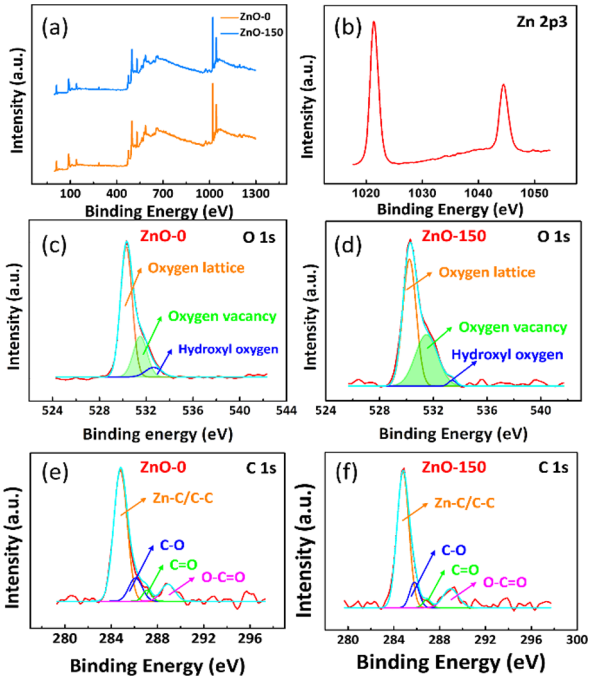

Figure 4. (a) Full-survey XPS spectra of ZnO-0 and ZnO-150. (b) High-resolution Zn 2p3 XPS spectra of ZnO-150. (c,e) High-resolution O 1s and C 1s XPS spectra of ZnO-0. (d,f) High-resolution O 1s and C 1s XPS spectra of ZnO-150.

deconvoluted into two peaks of Zn $2p_{3/2}$ and Zn $2p_{1/2}$, with the peaks centered at 1021.3 and 1044.5 eV, respectively (Figure 4b). It is in agreement with previously reported Zn 2p3 peak results.[23,27,28] Figure 4c,d presents the high-resolution O 1s spectra, which can be fitted to three Gaussian peaks. The dominant peak's binding energy is located at 530.2 eV, attributed to the presence of oxygen ions in the wurtzite-structured ZnO lattice. The second peak, located at 531.5 eV, can be assigned to oxygen vacancies (O^- and O^{2-} ions). The smallest peak located at 532.7 eV corresponds to chemisorbed hydroxyl groups at the nanostructure surface.[2,14,26,27] To further discuss the oxygen vacancy (V_O) defects in both devices, the V_O contents in ZnO-0 and ZnO-150 are 25.33 and 40.22%, respectively. The higher V_O defects, which possess a greater electron concentration, create more active sites and enhance sensing performance.[2,33−36] The C 1s spectra were fitted to four distinct peaks (Figure 4e,f), and the primary peak was centered at 284.8 eV, corresponding to Zn−C/C−C bonding. Additional peaks were observed at 285.8, 286.8, and 288.9, which can be attributed to C−O, C═O, and O−C═O functionalities, respectively. This indicates the presence of numerous oxygen-containing functional groups in the nanostructure.[23−25] Moreover, the carbon atomic percentages of ZnO-0 and ZnO-150 were 1.4 and 18.2%, respectively. With the apple pectin biotemplate, the carbon atomic percentage has

https://doi.org/10.1021/acsomega.3c07280
ACS Omega 2024, 9, 1077−1083

shown a dramatic increase, which plays a crucial role in the sensing performance.

The specific surface area and pore structure of the nanostructure were determined through N_2 adsorption/desorption measurements. The BET specific surface areas of ZnO-0 and ZnO-150 are 3.792 and 4.424 m^2/g, respectively. Figure 5a,b displays N_2 adsorption/desorption curves for both

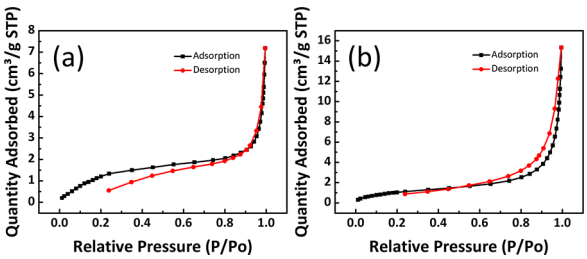

Figure 5. N_2 adsorption−desorption isotherms of (a) ZnO-0 and (b) ZnO-150.

ZnO-0 and ZnO-150, which exhibit reversible type IV isotherms and H_3-type hysteresis loops. The pore sizes (Figure 6a,b) of ZnO-0 and ZnO-150 are predominantly centered

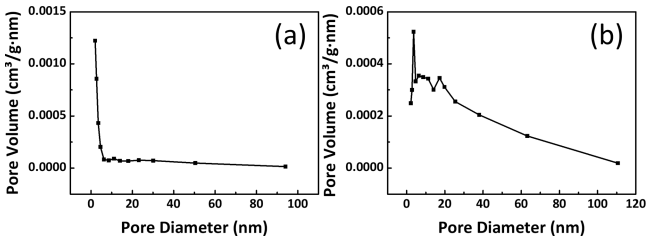

Figure 6. Pore size distributions of (a) ZnO-0 and (b) ZnO-150.

around 10.972 and 19.854 nm, respectively. The data results demonstrate that ZnO-150 possesses a higher surface-to-volume ratio.

To investigate the effect of operating temperature on the device's performance, resistance and response analyses were conducted at different temperatures with 350 ppb NO_2. The objective was to identify the optimal operating temperature for the device. The resistance in ambient air (R_{air}) value decreased as the operating temperature increased. This behavior can be attributed to the semiconductor conduction characteristics, where the higher temperatures result in increased electron concentration and excitation to the conduction band (Figure 7a).[13,14,29] Figure 7b−d illustrates the response analyses of both sensor devices. The response increased with temperature, reaching its highest response at 150 and 180 °C, indicating optimal adsorption and desorption capabilities. The responses of ZnO-150 and ZnO-0 at 150 °C were 2005.92 and 609.84%, respectively. The improved response at higher temperatures can be attributed to the availability of sufficient thermal energy for electron transitions to the conduction band, thereby enhancing the rate of adsorption capacity. However, excessively high operating temperatures (>150 °C) decreased response, attributed to increased gas adsorption and desorption on the sensing layer surface.[7] Due to the ZnO-150 response exceeding 100% at room temperature, the subsequent discussions will primarily focus on measurements conducted under ambient conditions.

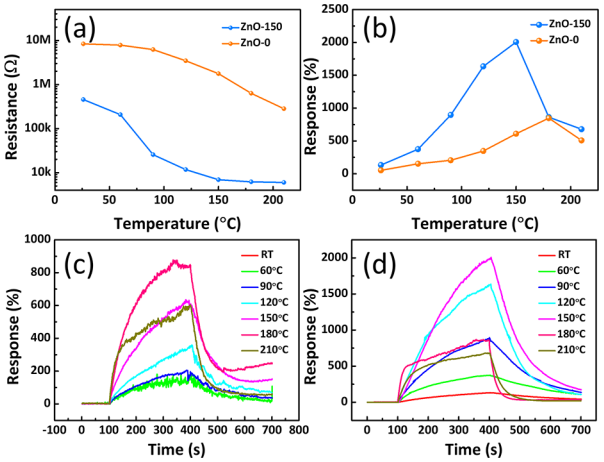

Figure 7. Comprehensive analysis of ZnO-0 and ZnO-150 for 350 ppb NO_2 at temperatures ranging from room temperature to 210 °C, (a) resistance value (R_{air}), (b) response, (c) response-recovery profile of ZnO-0, and (d) response-recovery profile of ZnO-150 with 350 ppb NO_2 at temperatures ranging from room temperature to 210 °C.

The gas sensing performances of ZnO-0 and ZnO-150 modified with the apple pectin biotemplate have been systematically investigated. Comparing apple pectin biotemplates reveals its potential as a strategy for modifying nanostructures. The response-recovery curve of apple pectin to variations in 350 ppb NO_2 at room temperature is presented in Figure 8a. The analyte gas (NO_2) was introduced for 5 min, and after that, the gas was removed, allowing the sensor response to fully recover over various time intervals. The

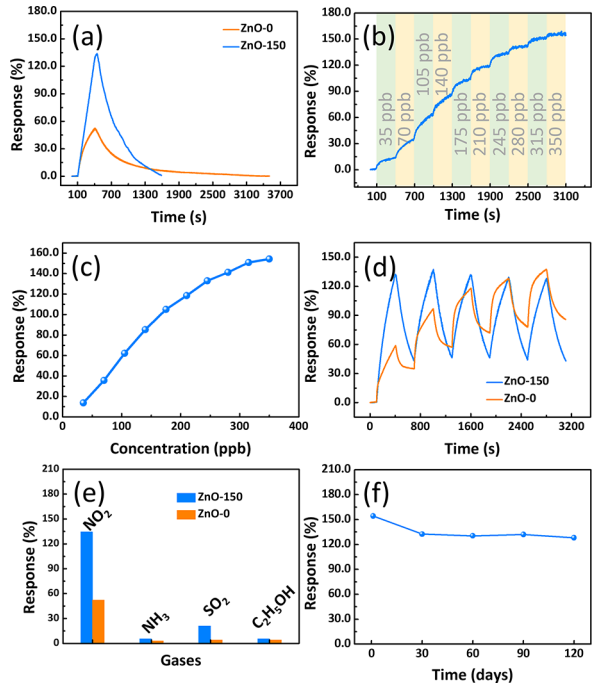

Figure 8. (a) Response-recovery profiles toward 350 ppb NO_2 of ZnO-0 and ZnO-150 at room temperature. (b) Sensitivity of ZnO-150 from 35 to 350 ppb and (c) response value as a function of different NO_2 concentrations. (d) Repeatability and reversibility of the sensor devices with five cycles. (e) Selectivity of sensor response with NO_2, C_2H_5OH, NH_3, and SO_2 at 350 ppb. (f) Long-term stability of ZnO-150 at 350 ppb NO_2.

https://doi.org/10.1021/acsomega.3c07280
ACS Omega 2024, 9, 1077−1083

sensor device utilizing ZnO-150 modified with the apple pectin biotemplate demonstrated a higher response of 132.44% compared to ZnO-0 (52.53%), approximately 2.52 times higher than that of ZnO-0. The response time for ZnO-150 is 231.7 s, with a recovery time of 732.5 s, whereas ZnO-0 exhibits a response time of 246.0 s and a recovery time of 1233 s in comparison. These results indicate that ZnO-150 shows a rapid performance in detecting NO_2 gas. The devices demonstrated low resistance in air atmospheres. However, the introduction of oxidizing NO_2 into the chamber resulted in an increase in resistance. This observation suggests that the sensing materials retain their n-type MOS characteristics, despite the incorporation of the apple pectin biotemplate for nanostructure modification and the attachment of plenty of C and N materials. The enhanced performance of ZnO-150 is hypothesized to be attributed to a higher surface-to-volume ratio and the presence of adsorbed C on the surface morphology. The sensitivity performance of ZnO-150 was evaluated by exposing them to NO_2 concentrations ranging from 35 to 350 ppb, as shown in Figure 8b,c. The obtained results exhibited an increasing response trend as the NO_2 concentration increased. The gas concentration increased by 35 ppb each time. ZnO-150 exhibited a remarkable response to trace 35 ppb NO_2 at room temperature, with a response of 13.74%. Interestingly, the response data are fitted by using two equations. For lower NO_2 concentrations (35−175 ppb), a linear equation fits remarkably well ($y = -9.294 + 0.663x$), yielding a high correlation coefficient ($R^2 = 0.997$). Meanwhile, at higher concentrations (175−350 ppb), an exponential equation fits exceptionally well ($y = -240.293 \times \exp(-x/146.736) + 177.370$), with a correlation coefficient of $R^2 = 0.993$. This highlights the device's exceptional capability to discriminate between various concentration levels and even detect trace amounts of NO_2.

To evaluate the repeatability and reversibility of the devices, multiple dynamic response measurements were performed. Figure 8d illustrates the comparison between ZnO-150 and ZnO-0, demonstrating the superior repeatability of the former over 5 cycles of exposure to 350 ppb NO_2 at room temperature. The average response for the ZnO-150 was 131.27%, with a corresponding standard deviation of 2.63%. Comparing with other gas sensors based on ZnO using biotemplates, it is worth noting that ZnO-150, synthesized with an apple pectin biotemplate, demonstrates an excellent NO_2 detection ability at room temperature.[2,30−34]

To verify the device's capability of discriminating the target gas in the presence of various interfering gases, response measurements were performed to assess the selective response of the device to different gases. As shown in Figure 8e, the responses of ZnO-0 and ZnO-150 to 350 ppb concentrations of NO_2, C_2H_5OH, NH_3, and SO_2 were measured at room temperature. The obtained response values were 132.44/52.53, 5.49/3.03, 5.54/3.99, and 21.06/4.25, respectively. Notably, the sensor device incorporating apple pectin-modified ZnO-150 exhibited a better selectivity coefficient (K_{AB} = $response_{NO2}/response_{SO2}$) of 6.29. The outstanding selectivity of the ZnO-150 sensor can be attributed to two main factors. First, the abundance of V_O defects in the ZnO-150 structure increases electron concentration, creating more active sites that enhance sensing performance.[2,32,35] Second, the strong electronic affinity of NO_2 (2.27 eV) results in a higher tendency to capture electrons from the sensing layer. These combined mechanisms contribute to ZnO-150's exceptional selectivity in detecting NO_2 gas.[2,31]

The ZnO-150 modified with apple pectin exhibits excellent performance in terms of response, sensitivity, selectivity, and repeatability. To verify the sensor's stability for environmental monitoring, the aging rate of the device was tested as an indicator of stability. Long-term stability of the ZnO-150 was evaluated at room temperature with 350 ppb NO_2, with measurements taken every 30 days, as shown in Figure 8f. After 120 days, the device exhibited minimal changes in response, with an average response value of 135.4% and a standard deviation of less than 9.54%. This indicates that the device maintains long-term stability under atmospheric conditions, making it suitable for prolonged monitoring.

The gas sensor mechanism of the MOS material can be described in terms of ionosorption behavior. The interaction between oxygen species and the analyte gas occurs through surface adsorption and desorption, which subsequently modulates the charge carrier concentration and the surface depletion region. These processes play a crucial role in controlling the resistance of the sensor. The ZnO semiconductor material inherently exhibits n-type characteristics due to its higher concentrations of donors. In ambient air environments, oxygen molecules are absorbed onto the surface and interact with electrons from the conduction band, resulting in the adsorption of several ionized oxygen species (O_2^-, O^{2-}, and O^-) on the surface of ZnO-150. The depletion layer is formed on the surface of the sensing material surface. At room temperature, the predominant one of the oxygen species is O_2^-, which leads to a decrease in conductivity. It can be described by the following equation (eq 2):

$$O_2(\text{abs}) + e^- \rightarrow O_2^- \quad (2)$$

After the interaction and contact of the ZnO-150 device with oxidizing NO_2, the electrophilic nature of NO_2 extracts electrons from the conduction band, resulting in the formation of NO_2^-. This causes a sharp increase in the resistance of the sensing material due to the widening depletion layer, as presented in the following equations (eqs 3 and 4):[28,36,37]

$$NO_2(\text{gas}) + e^- \rightarrow NO_2^-(\text{ads}) \quad (3)$$

$$NO_2(\text{ads}) + 2e^- + O_2^-(\text{ads}) \rightarrow NO_2^-(\text{ads}) + 2O^- \quad (4)$$

When the oxidizing NO_2 exits the chamber, it is replaced by air. Simultaneously, the NO_2 molecules will compete with the air molecules for the adsorption sites. The electrons will be released back to the conduction band, narrowing the depletion region. Consequently, the conductivity of the sensing material will gradually increase, contributing to a decrease in resistance.

In addition, the hydrothermal solution incorporating an apple pectin biotemplate successfully facilitated the attachment of carbon elements to the surface of the nanospheres. This process modified the nanostructure morphology, increasing the surface-to-volume ratio and generating sufficient active sites to enhance the capacity for chemisorbing oxygen.[6,19]

The crystallinity was also calculated from the XRD spectra (Figure 3a). ZnO-0 (85.36%) exhibits a much higher crystallinity compared to ZnO-150 (68.85%). According to previously published reports, n-type MOS materials with a lower crystallinity tend to have higher electron concentrations. Therefore, the resistance behavior of ZnO-150 exhibits a lower R_{air}, indicating that ZnO-150 has a higher NO_2 reaction ability and enhanced response.[38,39]

https://doi.org/10.1021/acsomega.3c07280
ACS Omega 2024, 9, 1077−1083

CONCLUSIONS

In this research, the successful utilization of apple pectin as a biotemplate via a facile hydrothermal method facilitated the growth of ZnO nanospheres. This nontoxic and environmentally friendly growth method not only modified the surface morphology to increase the surface-to-volume ratio but also enhanced the attachment of carbon elements to the nanostructures. Moreover, using an apple pection biotemplate for ZnO-150 generated abundant V_O defects (ZnO-0, 25.33%; ZnO-150, 40.22%), which possess a higher electron concentration, serving as active sites to enhance the adsorption capacity, especially toward the electrophilic nature of NO_2 gas. In comparison to unmodified zinc oxide nanorods (ZnO-0), the crystallinity of the apple pectin-modified ZnO-150 decreased from 85.36 to 68.85%, leading to an also increased surface electron concentration and enhanced gas response capabilities. The comprehensive enhancement mechanisms have led to an exceptional response of ZnO-150 toward 350 ppb NO_2 detection at room temperature, achieving a response rate of 132.44%. Even at trace concentrations as low as 35 ppb, it maintained good sensitivity at 13.74%. Furthermore, the nanostructure exhibited excellent repeatability over five cycles with no significant change (with a standard deviation of 2.63%), excellent selectivity (selectivity coefficient of 6.23%), and long-term stability for 120 days (standard deviation of less than 9.54%). These characteristics highlight its promising application potential. Therefore, the utilization of apple pectin as a biotemplate for the growth of ZnO-150 holds great promise as a potential candidate for room-temperature NO_2 detection.

AUTHOR INFORMATION

Corresponding Author

Yu-Chi Chang − *Department of Engineering Science, National Cheng Kung University, Tainan City 701, Taiwan (R.O.C.);* orcid.org/0000-0003-2253-935X; Email: christina780712@gmail.com

Authors

Jia-Cheng Jian − *Institute of Microelectronics, Department of Electrical Engineering, National Cheng Kung University, Tainan City 701, Taiwan (R.O.C.);* orcid.org/0000-0002-6277-6088

Sheng-Po Chang − *Department of Microelectronics Engineering, National Kaohsiung University of Science and Technology, Kaohsiung City 807, Taiwan (R.O.C.);* orcid.org/0000-0002-4126-0576

Shoou-Jinn Chang − *Institute of Microelectronics, Department of Electrical Engineering, National Cheng Kung University, Tainan City 701, Taiwan (R.O.C.)*

Complete contact information is available at: https://pubs.acs.org/10.1021/acsomega.3c07280

Notes

The authors declare no competing financial interest.

ACKNOWLEDGMENTS

This research is sponsored by the National Science and Technology Council of Taiwan Grant NSTC-112-2636-E-006-002 and the Taiwan Semiconductor Research Institute Grant JDP112-Y1-029. Additionally, the authors would like to express their gratitude to Jui-Chin Lee of the Core Facilities Center at National Cheng Kung University for supporting the use of ESCA−XPS (ESCA000200).

REFERENCES

(1) World Health, A. *Health and the environment: addressing the health impact of air pollution*. World Health Organization: Geneva, 2015.

(2) Li, C.; Sun, Y.-Y.; Li, Y.-N.; Zhang, X.-F.; Deng, Z.-P.; Huo, L.-H.; Xu, Y.-M.; Gao, S. Low-temperature and high-response NO2 sensor based on oxygen vacancy-enriched ZnO tubes inherited from waste chestnut mesocarps. *Sens. Actuators, B* **2023**, *388*, No. 133838.

(3) Sun, K.; Zhan, G.; Zhang, L.; Wang, Z.; Lin, S. Highly sensitive NO2 gas sensor based on ZnO nanoarray modulated by oxygen vacancy with Ce doping. *Sens. Actuators, B* **2023**, *379*, No. 133294.

(4) Wang, D.; Han, C.; Zheng, C.; Fang, H.; Xu, D.; Zhao, H. Fabrication of a ppb-level NO2 gas sensor by sensitizing nanobundles assembled by In2O3 nanotubes with TiO2 quantum dots. *Sens. Actuators, B* **2023**, *387*, No. 133833.

(5) Kumar, S.; Lawaniya, S. D.; Agarwal, S.; Yu, Y.-T.; Nelamarri, S. R.; Kumar, M.; Mishra, Y. K.; Awasthi, K. Optimization of Pt nanoparticles loading in ZnO for highly selective and stable hydrogen gas sensor at reduced working temperature. *Sens. Actuators, B* **2023**, *375*, No. 132943.

(6) Saravanan, A.; Huang, B.-R.; Kathiravan, D.; Prasannan, A. Natural biowaste-cocoon-derived granular activated carbon-coated ZnO nanorods: a simple route to synthesizing a core−shell structure and its highly enhanced UV and hydrogen sensing properties. *ACS Appl. Mater. Interfaces* **2017**, *9* (45), 39771−39780.

(7) Chen, M.; Wang, Z.; Han, D.; Gu, F.; Guo, G. High-sensitivity NO2 gas sensors based on flower-like and tube-like ZnO nanomaterials. *Sens. Actuators, B* **2011**, *157* (2), 565−574.

(8) Duoc, V. T.; Hung, C. M.; Nguyen, H.; Duy, N. V.; Hieu, N. V.; Hoa, N. D. Room temperature highly toxic NO2 gas sensors based on rootstock/scion nanowires of SnO2/ZnO, ZnO/SnO2, SnO2/SnO2 and, ZnO/ZnO. *Sens. Actuators B: Chem.* **2021**, *348*, No. 130652.

(9) Zhang, S.; Song, P.; Sun, J.; Ding, Y.; Wang, Q. MoO3/Ti3C2Tx MXene nanocomposites with rapid response for enhanced ethanol-sensing at a low temperature. *Sens. Actuators, B* **2023**, *378*, No. 133216.

(10) Zhang, S.; Song, P.; Wang, Q.; Ding, Y. Ultra-sensitive triethylamine gas sensor based on ZnO/MoO3 heterostructures with ppb level detection. *Sens. Actuators, B* **2023**, *379*, No. 133239.

(11) Chen, X.; Shen, Y.; Zhou, P.; Zhong, X.; Li, G.; Han, C.; Wei, D.; Li, S. Bimetallic Au/Pd nanoparticles decorated ZnO nanowires for NO2 detection. *Sens. Actuators, B* **2019**, *289*, 160−168.

(12) Li, Y.; Lv, T.; Zhao, F.-X.; Zou, Y.-L.; Lian, X.-X.; Zhou, Q.-J.; Liu, H.-P.; An, D.-M. Enhanced ethanol sensing and antibacterial activity of ZnO nanosheets synthesised using egg white as template. *Materials Technology* **2016**, *31* (4), 192−196.

(13) Liu, W.-X.; Sun, J.-B.; Li, Y.-N.; Kong, D.-R.; Song, B.-Y.; Zhang, X.-F.; Deng, Z.-P.; Xu, Y.-M.; Huo, L.-H.; Gao, S. Low-temperature and high-selectivity butanone sensor based on porous Fe2O3 nanosheets synthesized by phoenix tree leaf template. *Sens. Actuators, B* **2023**, *377*, No. 133054.

(14) Zhang, W.; Song, L.; Zhao, D.; Liu, T.; Jiang, H.; Yang, W.; Zhao, B.; Huang, W.; Wang, P.; Sui, L. Construction of hierarchical ZnO flower-like structure for boost H2S detection at low temperature. *Sens. Actuators, B* **2023**, *385*, No. 133728.

(15) Zhao, R.; Wang, Z.; Yang, Y.; Xing, X.; Zou, T.; Wang, Z.; Hong, P.; Peng, S.; Wang, Y. Pd-functionalized SnO2 nanofibers prepared by shaddock peels as bio-templates for high gas sensing performance toward butane. *Nanomaterials* **2019**, *9* (1), 13.

(16) He, H.; Zhao, C.; Xu, J.; Qu, K.; Jiang, Z.; Gao, Z.; Song, Y.-Y. Exploiting free-standing p-CuO/n-TiO2 nanochannels as a flexible gas sensor with high sensitivity for H2S at room temperature. *ACS sensors* **2021**, *6* (9), 3387−3397.

(17) Tsai, Y.-T.; Chang, S.-J.; Ji, L.-W.; Hsiao, Y.-J.; Tang, I. T.; Lu, H.-Y.; Chu, Y.-L. High Sensitivity of NO Gas Sensors Based on Novel

Ag-Doped ZnO Nanoflowers Enhanced with a UV Light-Emitting Diode. *ACS Omega* **2018**, *3* (10), 13798−13807.
(18) Cao, P. F.; Ma, S. Y.; Xu, X. L.; Wang, B. J.; Almamoun, O.; Han, T.; Xu, X. H.; Pei, S. T.; Zhang, R.; Zhang, J. L.; Liu, W. W. Preparation and characterization of a novel ethanol gas sensor based on FeYO3 microspheres by using orange peels as bio-templates. *Vacuum* **2020**, *177*, No. 109359.
(19) Kathiravan, D.; Huang, B.-R.; Saravanan, A. Multifunctional sustainable materials: the role of carbon existing protein in the enhanced gas and UV sensing performances of ZnO-based biofilms. *Journal of Materials Chemistry C* **2017**, *5* (21), 5239−5247.
(20) Prakash, T.; Jayaprakash, R.; Sathya Raj, D.; Kumar, S.; Donato, N.; Spadaro, D.; Neri, G. Sensing properties of ZnO nanoparticles synthesized by using albumen as a biotemplate for acetic acid monitoring in aqueous mixture. *Sens. Actuators B: Chem.* **2013**, *176*, 560−568.
(21) Saravanan, A.; Huang, B. R.; Kathiravan, D. Bio-industrial Waste Silk Fibroin Protein and Carbon Nanotube-Induced Carbonized Growth of One-Dimensional ZnO-based Bio-nanosheets and their Enhanced Optoelectronic Properties. Chemistry−A. *European Journal* **2018**, *24* (48), 12574−12583.
(22) Dakhlaoui, A.; Jendoubi, M.; Smiri, L. S.; Kanaev, A.; Jouini, N. Synthesis, characterization and optical properties of ZnO nanoparticles with controlled size and morphology. *J. Cryst. Growth* **2009**, *311* (16), 3989−3996.
(23) Chuang, C.-C.; Prasannan, A.; Huang, B.-R.; Hong, P.-D.; Chiang, M.-Y. Simple synthesis of eco-friendly multifunctional silk-sericin capped zinc oxide nanorods and their potential for fabrication of hydrogen sensors and UV photodetectors. *ACS Sustainable Chem. Eng.* **2017**, *5* (5), 4002−4010.
(24) Joshi, N.; da Silva, L. F.; Shimizu, F. M.; Mastelaro, V. R.; M'Peko, J. C.; Lin, L.; Oliveira, O. N. UV-assisted chemiresistors made with gold-modified ZnO nanorods to detect ozone gas at room temperature. *Microchim. Acta* **2019**, *186*, 1−9.
(25) Kwoka, M.; Kulis-Kapuscinska, A.; Zappa, D.; Comini, E.; Szuber, J. Novel insight on the local surface properties of ZnO nanowires. *Nanotechnology* **2020**, *31* (46), No. 465705.
(26) Fang, L.; Liu, J.; Ju, S.; Zheng, F.; Dong, W.; Shen, M. Experimental and theoretical evidence of enhanced ferromagnetism in sonochemical synthesized BiFeO3 nanoparticles. *Appl. Phys. Lett.* **2010**, *97* (24), 242501.
(27) Saravanan, A.; Huang, B.-R.; Kathiravan, D. Enhancement of UV Photodetection Properties of Hierarchical Core−Shell Heterostructures of a Natural Sericin Biopolymer with the Addition of ZnO Fabricated on Ultra-Nanocrystalline Diamond Layers. *ACS Appl. Mater. Interfaces* **2020**, *12* (2), 3254−3264.
(28) Li, Q.; Cui, Y.; Lin, J.; Zhao, C.; Ding, L. Synthesis of carbon microsphere-assisted snowflake-like ZnO nanomaterials for selective detection of NO2 at room temperature. *Journal of Industrial and Engineering Chemistry* **2022**, *110*, 542−551.
(29) Raju, P.; Li, Q. Semiconductor materials and devices for gas sensors. *J. Electrochem. Soc.* **2022**, *169* (5), No. 057518.
(30) Li, C.; Song, B.-Y.; Teng, Y.; Zhang, X.-F.; Deng, Z.-P.; Xu, Y.-M.; Huo, L.-H.; Gao, S. Biomass-derived hierarchical porous ZnO microtubules for highly selective detection of ppb-level nitric oxide at low temperature. *Sens. Actuators, B* **2021**, *333*, No. 129627.
(31) Li, C.; Sun, Y.-Y.; Lv, M.-S.; Zhang, X.-F.; Deng, Z.-P.; Xu, Y.-M.; Huo, L.-H.; Gao, S. Design Synthesis of ZnO Tube Bundles Rich in Oxygen Vacancies Assembled by Nanorods/Quasi-Nanospheres for Enhanced Sensing to NO/NO2. *ACS Sustainable Chem. Eng.* **2023**, *11* (16), 6405−6415.
(32) Lv, M.-S.; Li, C.; Li, Y.-N.; Zhang, X.-F.; Deng, Z.-P.; Cheng, X.-L.; Xu, Y.-M.; Huo, L.-H.; Gao, S. Facilely controlled synthesis of porous ZnO nanotubes with rich oxygen vacancies for highly sensitive and selective detection of NO2 at low temperature. *Sens. Actuators, B* **2023**, *375*, No. 132865.
(33) Lv, M.-S.; Li, Y.-N.; Chen, G.-L.; Gao, R.; Zhang, X.-F.; Deng, Z.-P.; Xu, Y.-M.; Huo, L.-H.; Gao, S. Biotemplate synthesis of NiO/ZnO tubes rich in oxygen vacancies for enhanced sensing detection of hydrazine at low temperature. *Sens. Actuators, B* **2023**, *385*, No. 133684.
(34) Na, H.-B.; Zhang, X.-F.; Zhang, M.; Deng, Z.-P.; Cheng, X.-L.; Huo, L.-H.; Gao, S. A fast response/recovery ppb-level H2S gas sensor based on porous CuO/ZnO heterostructural tubule via confined effect of absorbent cotton. *Sens. Actuators, B* **2019**, *297*, No. 126816.
(35) Kumar, R. R.; Murugesan, T.; Chang, T.-W.; Lin, H.-N. Defect controlled adsorption/desorption kinetics of ZnO nanorods for UV-activated NO2 gas sensing at room temperature. *Mater. Lett.* **2021**, *287*, No. 129257.
(36) Kang, S. B.; Sanger, A.; Jeong, M. H.; Baik, J. M.; Choi, K. J. Heterogeneous stacking of reduced graphene oxide on ZnO nanowires for NO2 gas sensors with dramatically improved response and high sensitivity. *Sens. Actuators, B* **2023**, *379*, No. 133196.
(37) Suganthi, K.; Vinoth, E.; Sudha, L.; Bharathi, P.; Navaneethan, M. Manganese (Mn2+) doped hexagonal prismatic zinc oxide (ZnO) nanostructures for chemiresistive NO2 sensor. *Sens. Actuators, B* **2023**, *380*, No. 133293.
(38) Katoch, A.; Sun, G.-J.; Choi, S.-W.; Byun, J.-H.; Kim, S. S. Competitive influence of grain size and crystallinity on gas sensing performances of ZnO nanofibers. *Sens. Actuators, B* **2013**, *185*, 411−416.
(39) Park, J. Y.; Kim, J.-J.; Kim, S. S. Electrical transport properties of ZnO nanofibers. *Microelectronic engineering* **2013**, *101*, 8−11.

https://doi.org/10.1021/acsomega.3c07280
ACS Omega 2024, 9, 1077−1083